Magnetic Resonance Imaging 55 (2019) 26–35

Contents lists available at ScienceDirect

Magnetic Resonance Imaging

journal homepage: www.elsevier.com/locate/mri

A correlative study between diffusion and perfusion MR imaging parameters on peripheral arterial disease data

Georgios S. Ioannidis[a,d,*,1], Kostas Marias[a,e], Nikolaos Galanakis[b,d], Kostas Perisinakis[a,c], Adam Hatzidakis[b], Dimitrios Tsetis[b], Apostolos Karantanas[a,b], Thomas G. Maris[a,c]

[a] Foundation for Research and Technology - Hellas (FORTH), Institute of Computer Science (ICS), Computational Bio-Medicine Laboratory (CBML), Heraklion, Greece
[b] Department of Medical Imaging, University of Crete, Heraklion, Greece
[c] Department of Medical Physics, University of Crete, Heraklion, Greece
[d] Medical School, University of Crete, Heraklion, Greece
[e] Technological Educational Institute of Crete, Department of Informatics Engineering, Heraklion, Greece

ARTICLE INFO

Keywords:
Dynamic contrast enhanced MR imaging
Diffusion weighted imaging
Peripheral arterial disease
Intravoxel incoherent motion
Mutual information (MI)
Pearson's correlation coefficient

ABSTRACT

Purpose: The purpose of this study was to correlate diffusion and perfusion quantitative and semi-quantitative MR parameters, on patients with peripheral arterial disease. In addition, we investigated which perfusion model better describes the behavior of the dynamic contrast-enhanced (DCE) MR data signal on ischemic regions of the lower limb.

Methods: Linear and nonlinear least squares algorithms, were incorporated for the quantification of the parameters through a variety of widely used models, able to extract physiological information from each imaging technique. All numerical calculations were implemented in Python 3.5 and include the: Intra voxel incoherent motion for diffusion and Patlak's, Extended Toft's and Gamma Capillary Transit time (GCTT) models for perfusion MRI.

Results: Our initial voxel by voxel correlation analysis didn't show any significant correlation based on the Pearson's Correlation metric between diffusion and perfusion parameters. To account for the inherited noise from the raw data, a Gaussian filter was applied to the parametric maps in order for the data to be comparable. By repeating our analysis in the filtered image maps, a good correlation (> 0.5) of diffusion and perfusion parameters was achieved.

Conclusions: Perfusion and diffusion MRI quantitative and semi-quantitative parameters can be obtained through a variety of physiological-pharmacokinetic models. This paper compares most of the widely-known models and parameters in both techniques with data from patients with peripheral arterial disease. Initial analysis showed no correlation in the perfusion parametric maps of DWI and DCE MRI data but a good correlation was obtained after smoothing the parametric maps indicating that perfusion information could be obtained from diffusion MRI images in patients with peripheral arterial disease.

1. Introduction

Dynamic contrast enhanced magnetic resonance imaging (DCE-MRI) is one of the most commonly used imaging techniques for measuring perfusion in biological tissues. DCE-MRI is based on acquiring a series of T1-weighted (T1W) images through time before and after the injection of exogenous gadolinium based contrast agent (CA) [1]. This procedure produces signal intensity time curves that after a suitable mathematical process and a selection of a proper model may provide information on vascular permeability, tissue perfusion, and expansions of extravascular- extracellular spaces (EES) [2].

Diffusion Weighted Imaging (DWI) is a technique that exploits the mobility of water molecules (molecular diffusion or Brownian motion) to produce signal on an MR image without contrast administration. A significant parameter that quantifies the degree of diffusion weighting (DW) applied is the b-value (in s/mm^2) which is mainly related with the

* Corresponding author at: Computational Bio-Medicine laboratory, Foundation for Research and Technology – Hellas, 100 Nikolaou Plastira str., Vassilika Vouton, Heraklion, Crete GR 700 13, Greece.
E-mail address: geo3721@ics.forth.gr (G.S. Ioannidis).
URL: http://www.ics.forth.gr/cbml/ (G.S. Ioannidis).
[1] Postal address: P.O. Box 1385, Heraklion, Crete GR - 711 10, Greece.

https://doi.org/10.1016/j.mri.2018.08.006
Received 26 January 2018; Received in revised form 7 August 2018; Accepted 14 August 2018

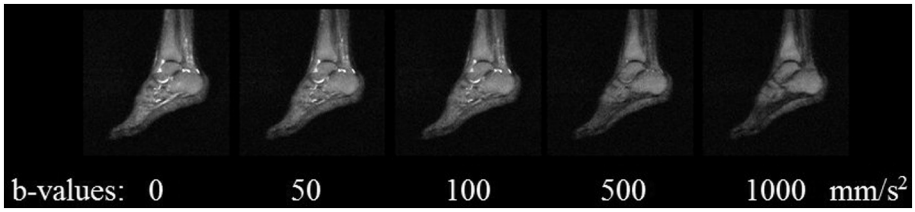

Fig. 1. DWI sequence of a central slice of the lower limb with 5 b values.

amplitude and time of the diffusion sensitizing gradients utilized on the MR scanner. The DW signal as a function of the b-value is considered to follow a mono-exponential decay providing the Apparent Diffusion Coefficient (ADC) (mm^2/s) [3]. In biological tissues, the mono-exponential model was not capable of analyzing the DW signal due to the presence of blood micro-circulation [4]. The micro-circulation of blood or micro-perfusion was considered to follow a Brownian motion model due to the random organization of the capillary network. Le Bihan et al. suggested the Intra-Voxel Incoherent Motion (IVIM) model in order to take into account both the real diffusion of water and the micro-circulation of blood inside a voxel [4].

Fitting the IVIM model to the DWI data, provides information not only about water diffusivity but also about soft tissue perfusion. This advantage of the diffusion IVIM model leads to the clinical question of the possible correlation between perfusion parameters deriving from DWI and DCE-MRI and whether the former can provide reliable, clinically-useful tissue perfusion information.

Several published works have shown the positive correlation of perfusion information between DCE-MRI and DWI in different regions and pathologies of the human body such as brain malignancies, [5,6] breast cancer [7] and head and neck squamous cell carcinoma [8]. These studies have in common the aggressiveness of each cancer type and consequently high vascularity and perfusion. On the contrary, the study of low tissue perfusion has not been extensively examined. To this end, we employ DCE-MRI and DWI techniques as a preliminary step for perfusion quantification on patients with peripheral arterial disease (PAD). The targeted impact of this work concerns the potential extraction of perfusion information from DWI-MRI avoiding CA administration especially in cases of clinical or other contraindications.

To address the above issues the aim of this paper is to qualitatively show the linear relationship between parametric maps originating from various known models obtained by DWI and DCE-MRI techniques with the application of a Gaussian filter. This comparative study was applied to patients with severe PAD before any kind of treatment.

PAD is an atherosclerotic process that causes stenosis or occlusion on lower extremity arteries. The major risk factors for PAD include older age, diabetes mellitus, hypertension, hyperlipidemia and smoking [9]. Patients with PAD may be asymptomatic or develop intermittent claudication. Ischemic rest pain, gangrene or ischemic ulcers may represent severe complications of PAD, leading to critical limb ischemia (CLI) [10]. Patients with CLI are at a higher amputation risk and require immediate revascularization by means of surgical or endovascular procedures [11].

2. Materials and methods

2.1. Patient population

During a 2 year-year study period (2015–2017), 13 patients (8 males, 5 females) with PAD underwent MR examination of lower limb. The median age was 68 years (range 56–78 years). All patients presented with CLI and according to Fontaine classification [12], 4 patients had stage III and 9 patients stage IV PAD. Exclusion criteria were all common contraindications to MRI, like pacemakers, ferromagnetic implants and claustrophobia and contraindications for administration of Gadolinium contrast medium such us renal insufficiency and allergy to gadolinium. The study was approved by the local ethic committee and all patients signed informed consent prior to examination.

2.2. MRI protocol

Each of 13 patients underwent MR examination on a 1.5 T clinical MR Scanner (Vision/Sonata Hybrid system, Siemens, Erlangen, Germany) enforced with powerful gradients (Strength: 45 mT/m, Slew rate: 200 mT/m/ms), equivalent with those gradients operating on 3 T systems.

The imaging protocol, apart from the conventional sequences, included DWI and DCE-MRI quantitative techniques. DW sagittal images of the lower limb were acquired utilizing a high resolution HASTE (Half-Fourier Acquisition Single-shot Turbo spin Echo) sequence with diffusion sensitizing gradients with b-values (b = 0, 50, 100, 150, 200, 500, 800, 1000 s/mm^2), number of slices = 13, echo time (TE) = 105 ms, repetition time (TR) = 2000 ms, matrix size = 384 × 384, field of view (FOV) = 250 × 250, slice thickness = 5 mm. Additionally, a reverse polarization gradient technique was applied by acquiring two sets of sagittal DW images, each time altering the polarization direction of the frequency encoding gradient A-P and P-A (Anterior-Posterior) [13]. This technique has been applied for the reduction of machine related geometrical distortions or apparent distortions in signal intensities. The final calculated image was the mathematical average of the two aforementioned DW sets. An example for five b-values of a central slice is shown in Fig. 1.

T1W DCE perfusion MR imaging of the lower limb was performed by utilizing a 3D VIBE (volume interpolated breath hold examination) sequence in the sagittal plane with variable flip angles (FA = 5°,10°,15°, 20°, 25°, 30°) for the initial calculation of the parametric T1 maps. Consequently, an intravenous continual injection of the paramagnetic CA (Magnevist, Gadopentetate Dimeglumine, Bayer Healthcare, Bayer, 0.1 mmol/kg) was administered for approximately 1 min. The aforementioned T1W DCE VIBE perfusion sequence was continuously repeated for 10min (20 s temporal resolution) after the intravenous injection of the CA with the following imaging parameters: number of slices = 26, FA = 15°, TE = 2.73 ms, TR = 7.8 ms, matrix size = 512 × 512, FOV = 250 × 250 and slice thickness = 3 mm.

2.3. DWI-MRI analysis

The quantification of both diffusion and perfusion parameters was implemented in our platform using python 3.5 [14]. More specifically, all parametric maps were obtained with the use of a trust region reflective algorithm [15], suitable for solving nonlinear bound-constrained minimization problems as defined in SciPy library [16] (scipy.optimize.least_squares).

According to the IVIM, the DWI signal as a function of the b-value is expressed in Eq. (A.1). S(b) is the measured signal intensity at the current b-value and $S(0)$ is the measured signal intensity without diffusion gradient attenuation factor (typically a T2 image), D is the diffusion coefficient, D^* is the pseudo-diffusion coefficient and f is the micro-perfusion fraction denoting the ratio of water flowing in capillaries to the total water contained in a voxel.

The quantification of the DW signal with the IVIM model is mainly succeeded by two different fitting methods. The first method is a direct

estimation of the IVIM parameters using the aforementioned nonlinear fitting algorithm with the following constraints for each parameter:

$$f \in (0,1),\ D \in (0,5) \times 10^{-3} mm^2/s,\quad D^* \in (10{,}200) \times 10^{-3} mm^2/s.$$

The second method is relied on the fact that for b-values $>$ 200 s/mm^2 the micro-perfusion effect is eliminated and does not contribute to the DW signal decay [17]. Thus, in the high b-value range (b $>$ 200 s/mm^2) the signal attenuation is considered to be of the form of Eq. (A.2) and D is estimated by using a linear fit to Eq. (A.2) after taking the logarithm of both sides (scipy.optimize.lsq_linear). Once D is known, parameters f and D* are estimated from Eq. (A.1) by using the nonlinear fitting algorithm with the same bound constraints as in the first method for all available b-values.

2.4. DCE-MRI analysis

The procedure for the quantification of the DCE-MRI signal has two important steps [18]. First, the concentration curve as a function of time of the CA is computed ($C_t(t)$) and then, after the choice of a suitable pharmacokinetic model, nonlinear fitting of the concentration curve is required in order to produce tissue perfusion parameters.

The linear relationship between the relaxation rates ($R_1 = 1/T_1$, $R_{10} = 1/T_{10}$) and the CA concentration (c) in the tissue is given by Eq. (A.3). T_{10} is the relaxation time of tissues before the injection of CA and T_1 after the injection of CA and $r_1 \approx 4.5\,s^{-1}\,mM^{-1}$ is the ratio of CA concentration to the increase in relaxation rate R_1 measured at 1.5 T.

The signal (S) of the variable flip angle (θ) sequence before the injection of the CA, is given by Eq. (A.4) [19] with TR = 7.8 ms from the imaging protocol. S_0 is the relaxed signal. Therefore, both S_0 and T_{10} were fitted to Eq. (A.4) with bound constraints $S_0 \in (1{,}10.000)$, $T_{10} \in (0,5)$ ms. Thus, for every voxel in time, the concentration curve was calculated from Eq. (A.3) after solving for T_1 on Eq. (A.4).

In order to provide information about tissue perfusion to patients with PAD a variety of pharmacokinetic models were used such as, the extended Tofts model (ETM) [20], the Patlak model (PM) [21], the steady state model (SSM) [22] and the Gamma capillary transit time model (GCTT) [23].

ETM is the most widely used model for the analysis of DCE MRI data [24] and describes a highly perfused tissue with the assumption of a bidirectional transfer of the CA between the blood plasma and the EES. Mathematically, the model is described by Eq. (A.5).

The symbol $\circledast$ represents the convolution operator, $K^{Trans}\ min^{-1}$ is the transfer constant from the blood plasma into the EES and $K_{ep} min^{-1}$ is the transfer constant from the EES back to the blood plasma while v_p stands for the plasma volume and $C_a(t)$ for the time concentration curve of a feeding artery, also known as the arterial input function (AIF). In our case, the AIF was the same for all perfusion models and selected carefully by clinicians from the posterior tibial artery. The selection of the AIF and the AIF curve over time is shown in Fig. 2.

A special case of the ETM when there is no transfer of CA from the EES back to blood plasma is the PM and it is given by Eq. (A.6). In addition, if it is assumed that there is no transfer of CA from the blood plasma into the EES, the SSM model is acquired, indicating that the concentration of the feeding artery and the tissue concentration are in a state of equilibrium. The one parameter SSM is presented by Eq. (A.7).

Except from its complex form, the GCTT model was included in this study since it is a more recently suggested physiological model unifying well-known models such as the Tofts Model [25],the ETM, the adiabatic tissue homogeneity (ATH) model [26] and the two compartment exchange (2CX) model [27]. The GCTT model is presented in Eq. (A.8). F $mL/mL/min^{-1}$is the blood flow or blood perfusion, $a^{-1} = t_c/\tau$ is the width of the distribution of the capillary transit times inside a voxel, $\gamma(a,z)$ is the gamma function, E is the extraction fraction of CA that is extracted into the EES during a single capillary transit.

Except from the previous models, two semi quantitative parameters were also calculated from the signal intensity curve over time $SI(t)$ such as the area under the curve (AUC) and the relative enhancement ratio (RER) Eqs. (A.9) and (A.10) respectively.

2.5. Statistical analysis

In this work, two statistical metrics were used, the adjusted R squared ($\overline{R}^2$) and the root mean squared error (RMSE), to determine the goodness of fit for every voxel. Assuming that the model function is $G(x,t)$ with parameters $x = \{x_1, x_2, \ldots, x_p\}$ and N data points d the RMSE formula is given by Eq. (A.11).

$\overline{R}^2$ is a generalized metric that is based on the R squared (R^2) and its value will always be less than or equal to that of $\overline{R}^2 \in [0,1]$. This metric was proposed to overcome the limitation of R^2 concerning that its value increases when more explanatory variables are added to the model. Therefore, it was considered to be more suitable for this study than R^2 since it captures the number of data points (N) as well as the number of the explanatory variables (p) of the model function Eq. (A.12).

2.6. Correlation analysis

Firstly, to examine the relation between DWI and DCE-MRI data for every individual patient, perfusion parametric maps were resized through cubic interpolation to the size of the diffusion parametric maps. Pearson's r correlation coefficient was then calculated taking into account the slices from perfusion and diffusion sequences with the same slice location dicom tag, while rejecting all voxels from tissues without significant blood supply (non-perfused) such as the osseous structures ($v_p = 0$). To ensure that after resizing, the parametric maps are accurately registered in space, we performed two tests as shown in Fig. 8. The color-coded fusion of a DW image on a perfusion T1W image is presented and a Canny edge detector ($\sigma = 0.5$) [28] highlighted the edges of DCE T1W image which are then superimposed on the corresponding DW image. Both tests clearly demonstrated accurate alignment in all DWI, DCE-MRI image pairs used in our analyses according to senior radiologists involved in the study.

The effects of noise, after the fitting process, led to parametric maps that exhibit large variations within voxels in small neighborhoods (Fig. 6). Thus, in order to examine the relationship between DCE and DWI parameters in a more effective and qualitative way, a 5×5 Gaussian filter ($\sigma = 0.9$) was applied on the derived parametric maps.

2.7. Mutual information analysis

Except from the Pearson's Correlation metric and the consideration of the images (parametric maps) as random variables, we also calculated the Mutual Information (MI) of the previously described diffusion and perfusion parameters with and without Gaussian filter. Mutual information metric arises from information theory and measures how much one random variable (an image in our case) tells us about another [29]. MI is an alternative perspective of checking the correlation between different imaging techniques that does not take into account only pixel values such as Pearson's correlation but also the entropy of the image pair.

Considering two discrete random variables X and Y of size N with their mass probability functions p(X), p(Y) and with their joint probability mass function p(x, y) it is possible to calculate their mutual information. On our case the random variables (X,Y) are (f,vp). Prior to the definition of the mutual information it is obligatory to define the entropy of a random variable X which is given by Eq. (A.13). Furthermore, the joint entropy H(X,Y) of a pair of discrete random variables (X,Y) with a probability mass function p(x,y) is given by Eq. (A.14). Having the formulae of the entropies above, the MI is calculated by Eq. (A.15) [30].

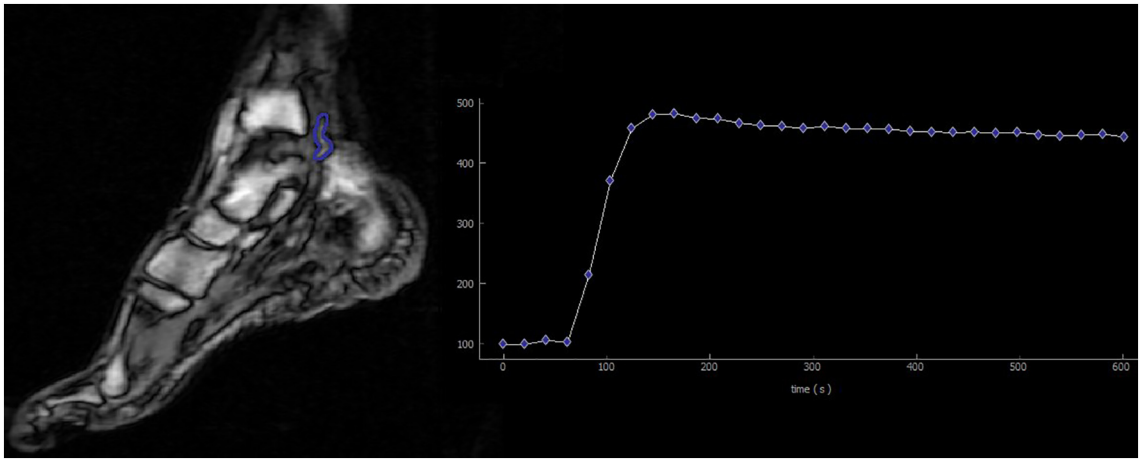

Fig. 2. The blue ROI of the AIF is shown on the T1W image of perfusion sequence (left) and its curve over time on the plot (right). (For interpretation of the references to color in this figure legend, the reader is referred to the web version of this article.)

2.8. Signal to noise ratio (SNR)

A significant factor about image quality is SNR. In our study, SNR was calculated by Eq. (A.16) in which, mean(SI_{ROI}) is the mean signal intensity from the selected region of interest (ROI) and std(BG_{ROI}) is the standard deviation of a background ROI which was meticulously taken outside of the depicted image volume avoiding any prominent artifact. Since the recorded signals from the BG_{ROI} follow a Rayleigh rather than a Gaussian distribution, the SNR value was multiplied by the correction factor 0.655 [31]. For every patient, SI_{ROI} was selected from the whole anatomical image of the central slice. The calculated SNR for DW images was graphically presented as a box and whisker plot for every b-value (Fig. 3). The calculated SNR for the variable flip angle Proton Density weighted (PDW) and T1W images is shown in Fig. 4. Finally, the calculated SNR for the perfusion weighted images was calculated for three time points, the one before the injection of the CA (Baseline), the time at the Maximum signal from the signal intensity curve (time to peak TTPK) and at the last time point of the perfusion sequence as is shown in Fig. 5. Every box and whisker plot contains the calculated SNR for every patient.

3. Results

3.1. DWI and DCE MRI fitting performance

Metrics from the statistical analysis, showed that regarding the DWI fitting, both the first and the second fitting method were quite accurate since RMSE and $\overline{R}^2$ were as expected at the desired levels, meaning low RMSE and high $\overline{R}^2$. More precisely, for the first fitting method, RMSE = 0.081 ± (0.048), $\overline{R}^2$ = 0.637 ± (0.292) and for the second method, RMSE = 0.085 ± (0.05), $\overline{R}^2$ = 0.627 ± (0.285). DCE MRI statistical metrics for each perfusion model are shown in Table 1. A graphical representation of each aforementioned model fit in a region of the peroneus brevis muscle for DWI and DCE-MRI is depicted in Fig. 9 and Fig. 10 respectively.

3.2. DWI and DCE MRI correlation

Pearson's correlation (r) coefficient was calculated for every perfusion and diffusion model-based parametric map. In Table 2, Pearson's correlation coefficient r, is presented between the parameter (f-IVIM) and the perfusion plasma volume parameters. A graphical illustration of the normalized parametric maps is depicted in Fig. 6. Analogously, r after the application of the Gaussian filter on the parametric maps is presented between (f-IVIM) and the perfusion parameters in Table 3

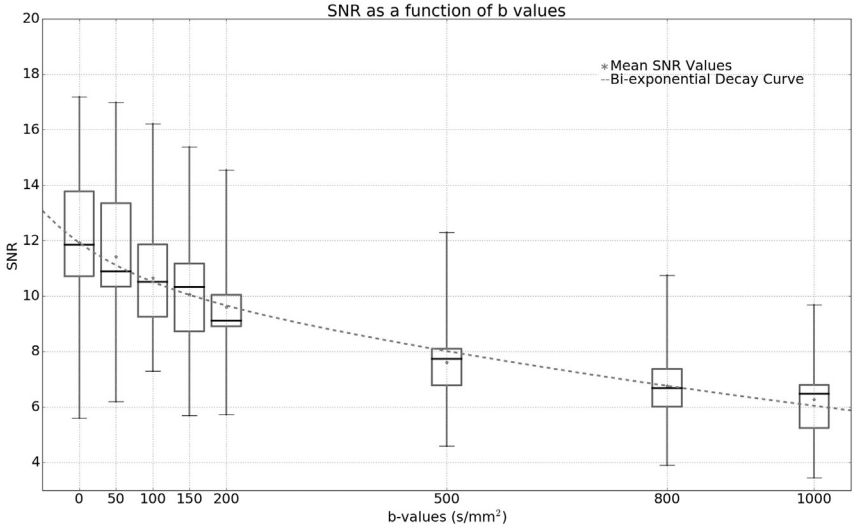

Fig. 3. SNR as a function of b-values for every patient. Star dots present the mean SNR value and the dotted line is the fitted IVIM function to the star dots.

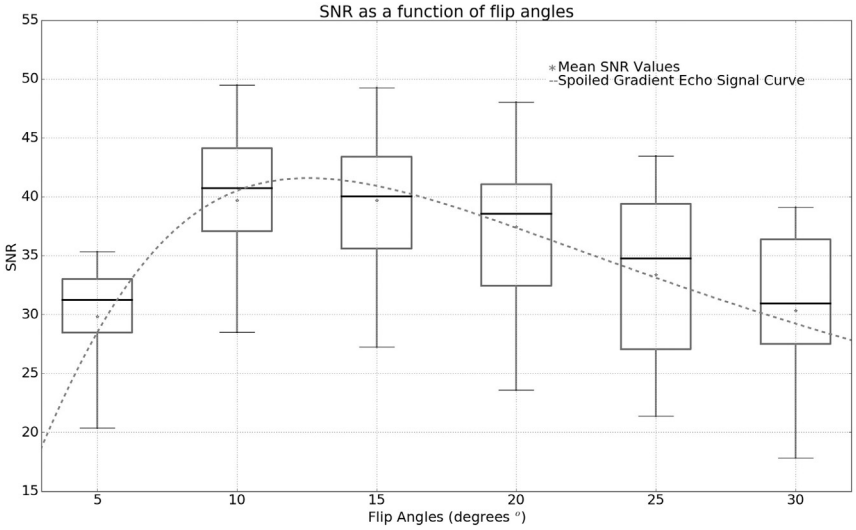

Fig. 4. SNR as a function of flip angles for every patient. Star dots present the mean SNR value and the dotted line is the fitted Eq. (A.4) to the star dots.

while the smoothed parametric maps are shown in Fig. 7. All p-values of the correlation analysis for both tables were lower than 0.05.

3.3. Mutual information analysis

As in the previous paragraph MI was calculated between f-IVIM (method 1) and the perfusion plasma volume parameters. The results for each model are depicted as boxplots before and after applying the Gaussian filter in Fig. 11.

4. Discussion and conclusions

The main goal of this study was to show the relationship between diffusion and perfusion related parameters. This constitutes a challenging goal since gadolinium based contrast agents are increasingly restricted due to effects on the human body according to EMA (European Medicines Agency) [32]. For this reason, the use of DWI taking advantage of its micro-perfusion instead of perfusion, is of outmost importance.

To the best of our knowledge, the majority of the published works on patients with PAD disease arterial spin labeling (ASL) and Blood oxygenation level-dependent (BOLD) MRI techniques are used [33–36]

Table 1
Perfusion statistical Metrics per model.

Fitting model	RMSE ± (std)	$\bar{R}^2$ ± (std)
SSM	0.033 ± (0.092)	0.126 ± (0.171)
PM	0.031 ± (0.091)	0.337 ± (0.316)
ETM	0.039 ± (0.101)	0.322 ± (0.321)
GCTT	0.029 ± (0.082)	0.143 ± (0.221)

Table 2
Pearson's Correlation coefficient r without Gaussian Filtering to the parametric maps.

Fitting model (parameter)	DWI-Method 1 (f)	DWI-Method 2 (f)
SSM (v_p)	0.082	0.086
PM (v_p)	0.073	0.071
ETM (v_p)	0.046	0.043
GCTT (E)	0.039	0.045
AUC	0.011	0.013
RER	−0.114	−0.107

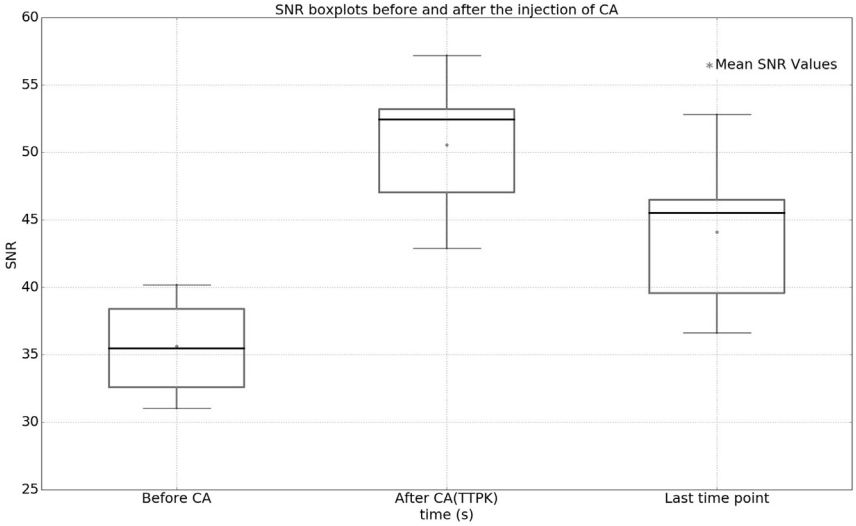

Fig. 5. SNR of the perfusion imaging sequence for three indicative time points (Baseline, TTPK, Last point of imaging sequence).

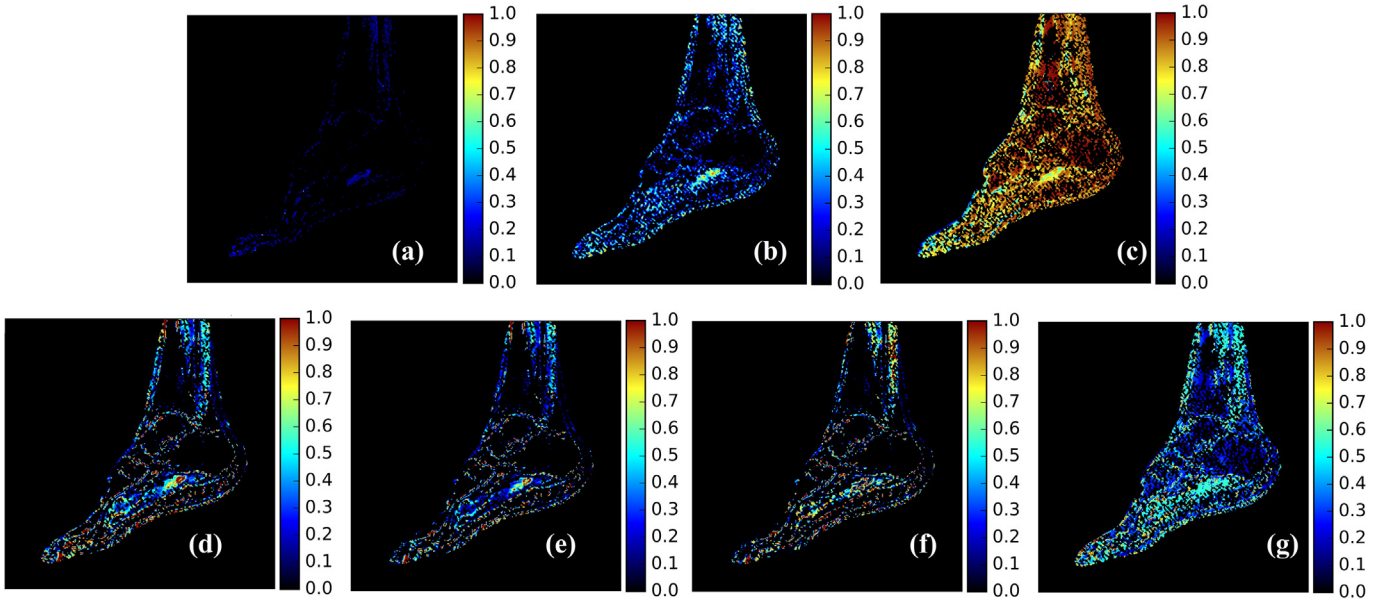

Fig. 6. Blood plasma volume related parametric maps. (b) f-IVIM, semi- quantitative: (a) RER and (c) AUC and (d)-(g) SSM (vp), PM (vp), ETM (vp), GCTT (E) respectively.

Table 3
Pearson's Correlation coefficient r with Gaussian Filtering to the parametric maps.

Fitting model (parameter)	DWI-Method 1 (f)	DWI-Method 2 (f)
SSM (v_p)	0.429	0.427
PM (v_p)	0.379	0.366
ETM (v_p)	0.406	0.397
GCTT (E)	**0.544**	**0.551**
AUC	0.254	0.252
RER	**0.592**	**0.601**

to quantify PAD disease. Moreover, DWI technique has not been used. Thus, a priori knowledge of quantitative results in PAD disease could not be possible to be compared with our results.

This paper examined the possible correlation between perfusion parameters derived from DWI and DCE-MRI and whether the former can provide robust and accurate information regarding perfusion of an individual anatomic region which in cases of PAD is clinically important.

To examine this possible correlation, we analyzed PAD data. The statistical metrics RMSE and $\overline{R}^2$ were used for both diffusion and perfusion models and were computed in all cases in order to enhance the reliability of the results. RMSE for diffusion fitting methods and perfusion models was (as expected) low and very similar (in order of magnitude) for all models due to the tolerance of the fitting algorithm (10^{-16}). Though, the dominant statistical metric that played a great role to our analysis was the strict metric $\overline{R}^2$ due to its ability to handle the number of data points and explanatory variables of each model.

Due to $\overline{R}^2$, it could be expected that the best and the most widely used model for perfusion imaging would be the extended Tofts model.

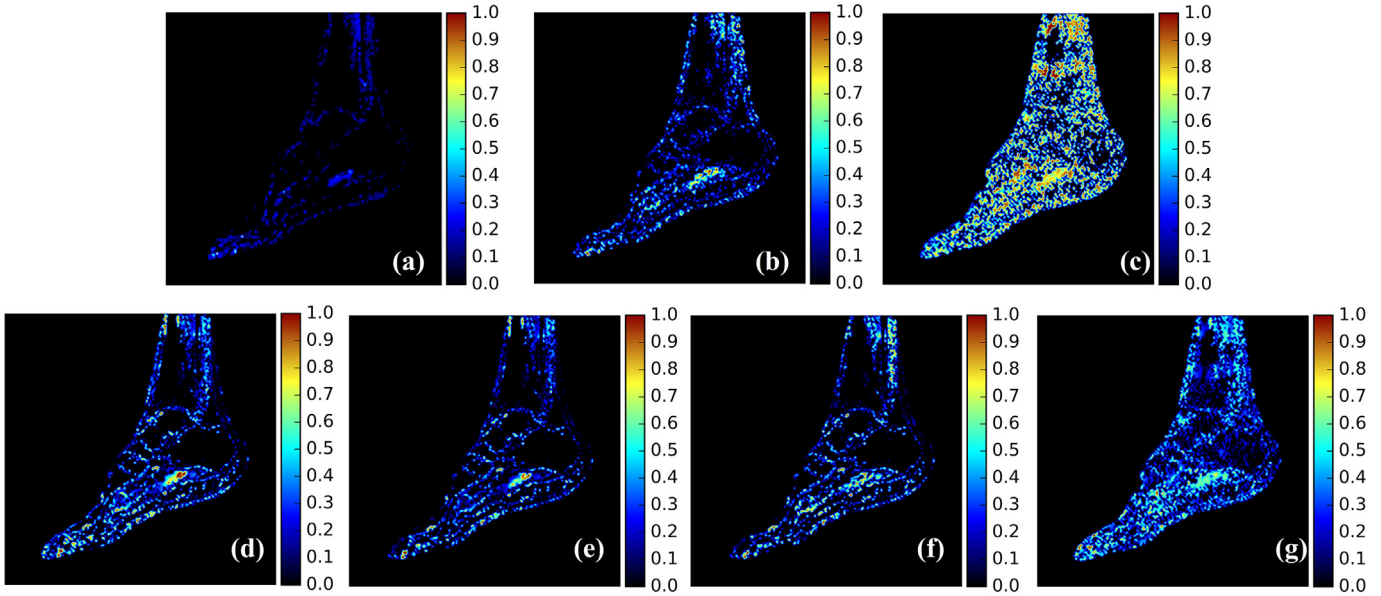

Fig. 7. Blood plasma volume related parametric maps after the application of a 5 × 5 Gaussian filter (σ = 0.9). (b) f-IVIM, semi- quantitative: (a) RER and (c) AUC and (d)-(g) SSM (vp), PM (vp), ETM (vp), GCTT (E) respectively.

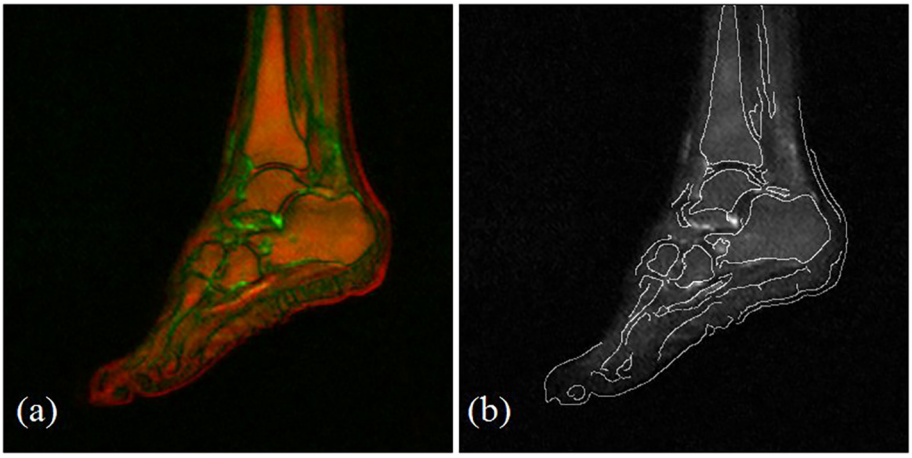

Fig. 8. (a) Color fusion of aligned DCE-MRI and DWI. Red color intensity indicates areas of high perfusion and green intensity represents high DWI signal. (b) T1W edges with Canny edge detector with σ = 0.5 superimposed on the DW corresponding image. (For interpretation of the references to color in this figure legend, the reader is referred to the web version of this article.)

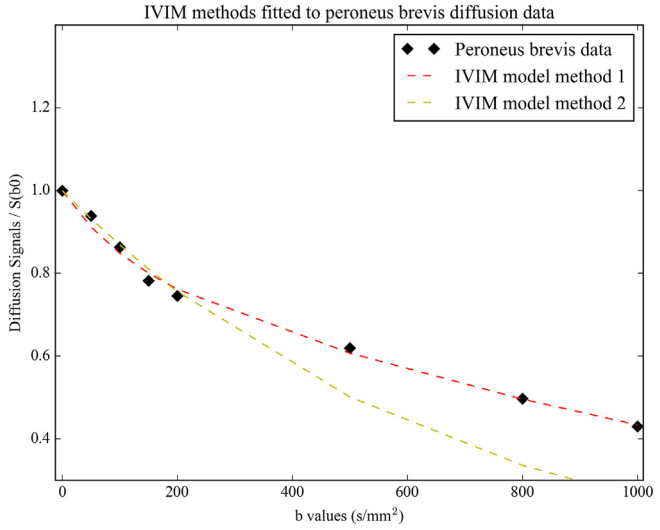

Fig. 9. IVIM model method 1 and 2 fitted to DWI data obtained from the peroneus brevis muscle.

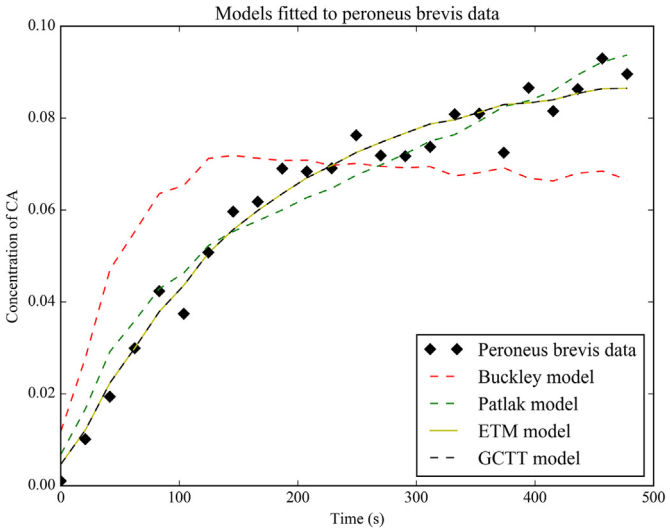

Fig. 10. Pharmacokinetic models fitted to DCE data derived from the peroneus brevis muscle.

On the contrary, Patlak's model achieved a little higher $\overline{R}^2$ than ETM (Table 1). This could be attributed to the PAD which causes stenosis or occlusion on lower extremity arteries. As mentioned earlier Patlak's model assumes no transfer of CA from the EES back to blood plasma, in contrast to ETM that assumes a bidirectional transfer of the CA between the blood plasma and the EES. Regarding to DWI, no significant differences on adjusted R2 values between IVIM fitting method 1 and method 2 were observed.

A variety of perfusion models quantitative and semi-quantitative and two diffusion analysis methods were used. The results of the standard fitting procedure (meaning no Gaussian filtering) showed no correlation at all because Pearson's r was close to zero. However, looking at the parametric maps, (Fig. 6) the visual inspection of the raw data confirmed the noise coming from the imaging process and led us to use the Gaussian filter for smoothing the parametric maps (Fig. 7) and removing the inherent noise. Subsequently, diffusion parameter f-IVIM on both diffusion methods was correlated well with GCTT-E ($r_{GCTT\ E-fmethod\ 1} = \mathbf{0.54}, r_{GCTT\ E-fmethod\ 2} = \mathbf{0.551}$) and with RER ($r_{RER-fmethod\ 1} = \mathbf{0.592}, r_{RER-fmethod\ 2} = \mathbf{0.601}$). These encouraging results point out the necessity for more thorough studies, possibly by utilizing MR scanners with higher field strengths and diffusion sensitizing gradients. Moreover, the use of HASTE or TSE sequences enforced with powerful fast switching diffusion sensitizing gradients and multiple b-values with higher ranges (> 2000) is an absolute necessity. The ultimate goal would be therefore, to reduce DCE-MR perfusion examinations by performing DWI micro-perfusion studies. This will eventually whittle the use intravenous injections of CA and increase the number of patient groups enrolling in such type of studies.

Furthermore, in all of our cases of the results from mutual information analysis (Fig. 11) we observed an increment in MI of image pairs greater than approximately 42% after the application of the Gaussian filter. This strongly indicates that Gaussian filtering significantly increases the similarity between DWI and DCE image pairs and explains the vast improvement in the perfusion correlation results.

Similar published works on different parts of the human body and diseases confirm our results and altogether add to the consistent correlation of DCE and DWI MRI perfusion maps. Kim et al. and Federau et al. on their research concerning quantitative parameters on brain malignancies report that f-IVIM and CBV from Dynamic Susceptibility Contrast MRI, were positively correlated with $r = 0.67$ and $r = 0.75$ respectively [5,6]. Furthermore, Suo et al. on their semi-quantitative perfusion DCE analysis on breast cancer with a 3 T MR scanner and by filtering the DCE data with a Gaussian filter, achieved a correlation between (f-IVIM) values and RER with $r = 0.55$ and (f-IVIM) values and AUC with $r = 0.56$ [7]. We appraise that possible reasons these two studies achieved better correlations than ours and Suo's et al., might be: the absence of macroscopic motion artifacts of the patient, the presence

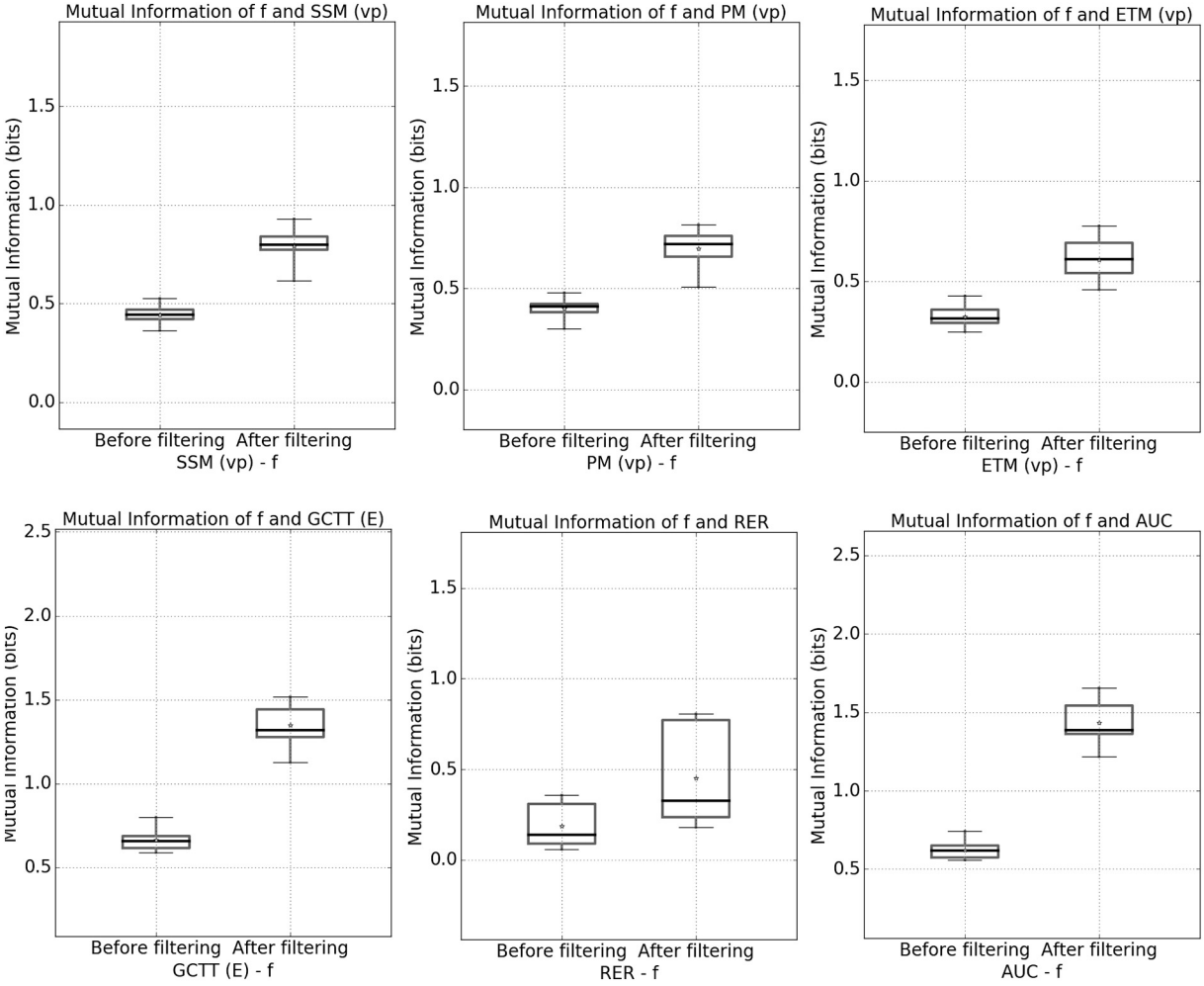

Fig. 11. Mutual information between f-IVIM method 1 and SSM (vp), PM (vp), ETM (vp), GCTT (E), RER, AUC before and after Gaussian filtering.

of anatomical barriers (membranes) in the brain that direct the anisotropic water diffusion and the reduced tissue perfusion due to PAD in our patients. In addition, another reason for the better correlation of Federau et al. could be attributed to their DWI experimental protocol consisting of 16 b-values ranging from 0 to 900 s/mm^2 that makes the diffusion measurement more precise.

The purpose of the clinical study in which this work is based, was to evaluate the perfusion of soft tissues in the foot of PAD patients. Thus, the relatively slow injection rate was chosen for two reasons. Firstly, muscles are normally characterized by slow perfusion rate which can be easily quantified using a slow injection rate. Secondly, the “bolus” injection technique induces susceptibility artifacts from the presence of highly concentrated contrast agent which in turn can be downgraded with the slow rate non-bolus administration. The low temporal resolution was chosen in order to compensate for the spatial covering of the imaging volume which has been previously reported in [37]. In fact, the total volume coverage was 26 space filling slices of 3 mm slice thickness. The selected volume coverage was considered adequate for the depiction of lower limb arteries and veins that might be related to blood supply to the ischemic regions of interest.

At this stage it is important to highlight the limitations of this study. The first limitation is that due to the clinical imaging protocol a good spatial resolution was chosen at the expense of a compromised SNR (matrix size 384 × 384) at the DW images. Additionally, in order to estimate the Pearson's correlation coefficient (r) through voxel by voxel analysis we had to resize the perfusion maps to match the size of the diffusion maps and this may have had a negative impact on the results. Regarding our dataset, it is noteworthy that it is limited to a relatively small subset of patients ($N = 13$) which means that further studies based on larger cohorts will be necessary for increasing the statistical significance of our results. Furthermore, the patients of the study presented with critical limb ischemia and some motion artifacts were observed especially in the perfusion imaging sequence (30 min approximately). To account for this, an idea for future work is to also use image registration which is hard due to the non-rigid nature of the transformation which might be affecting the results.

In conclusion, in this study we assessed different DWI and DCE-MRI analysis methods on data obtained from patients with PAD. According to $\overline{R}^2$ criterion we found that the best DWI fitting method was the direct estimation of the IVIM parameters (first method) and the most accurate perfusion model for this disease was the Patlak's model. Initially, IVIM parameters did not correlate with any of the perfusion parameters (quantitative and semi-quantitative) but, after the application of Gaussian filtering, a positive correlation between the extraction fraction E (GCTT) and RER with the micro-perfusion fraction (IVIM) with both of the DWI fitting methods rGCTTE − fmethod = 0.54, rGCTTE − fmethod = 0.551, rRER − fmethod = 0.592, rRER − fmethod = 0.601was obtained. Our results indicate that diffusion IVIM analysis could provide reliable information about tissue micro-perfusion and can be easily incorporated as a part of a conventional imaging clinical MRI protocol.

Acknowledgements

This work was supported by the General Secretariat for Research and Technology (GSRT) and the Hellenic Foundation for Research and Innovation (HFRI).

Appendix A. Formulae and equations

$$S(b)/S(0) = (1-f)e^{-bD} + fe^{-bD^*} \tag{A.1}$$

$$S(b)/S(0) = e^{-bD} \tag{A.2}$$

$$\frac{1}{T_1} = \frac{1}{T_{10}} + r_1 c \tag{A.3}$$

$$\frac{S}{S_0} = \frac{(1-e^{-TR/T_1})sin\theta}{1-e^{-TR/T_1}cos\theta} \tag{A.4}$$

$$C_t(t) = K^{trans} e^{-K_{ep}t} \circledast C_a(t) + v_p C_a(t) \tag{A.5}$$

$$C_t(t) = K^{trans} \int_0^t C_a(\tau)d\tau + v_p C_a(t) \tag{A.6}$$

$$C_t(t) = v_p C_a(t) \tag{A.7}$$

$$C_t(t) = F\left[\gamma\left(\frac{1}{a^{-1}}, \frac{t}{\tau}\right) + \frac{Ee^{-K_{ep}t}}{(1-K_{ep}\tau)^{1/a-1}}\left[1-\gamma\left(\frac{1}{a^{-1}}, \left(\frac{1}{\tau}-K_{ep}\right)t\right)\right]\right] \circledast C_a(t) \tag{A.8}$$

$$AUC = \int_0^t SI(\tau)d\tau \tag{A.9}$$

$$RER = \frac{SI_{post} - SI_{pre}}{SI_{pre}} \tag{A.10}$$

$$RMSE = \sqrt{\sum_{i=1}^{N} \frac{(G(x,t_i) - d_i)^2}{N}} \tag{A.11}$$

$$\overline{R}^2 = 1 - (1-R^2)\frac{N-1}{N-p-1} \tag{A.12}$$

$$H(X) = -\sum_{x \in X} p(x)\log(p(x)) \tag{A.13}$$

$$H(X,Y) = -\sum_{x \in X}\sum_{y \in Y} p(x,y)\ \log(p(x,y)) \tag{A.14}$$

$$\mathrm{MI}(\mathrm{X},\mathrm{Y}) = \mathrm{H}(\mathrm{X}) + H(Y) - H(X,Y) \tag{A.15}$$

$$\mathrm{SNR} = \frac{\mathrm{mean}(\mathrm{SI_{ROI}})}{\mathrm{std}(\mathrm{BG_{ROI}})} \times 0.655 \tag{A.16}$$

References

[1] Choyke PL, Dwyer AJ, Knopp MV. Functional tumor imaging with dynamic contrast-enhanced magnetic resonance imaging. J Magn Reson Imaging 2003;17:509–20. https://doi.org/10.1002/jmri.10304.
[2] Essig M, Shiroishi MS, Nguyen TB, Saake M, Provenzale JM, Enterline D, et al. Perfusion MRI: the five most frequently asked technical questions. 2013. https://doi.org/10.2214/AJR.12.9543.
[3] Hagmann P, Jonasson L, Maeder P, Thiran J, Wedeen VJ, Meuli R. Central nervous system: state of the art understanding diffusion MR imaging techniques: from scalar imaging to diffusion. Radiographics 2006:205–24.
[4] Le Bihan Denis, Eric Breton DL. Seperation of diffusion and perfusion in intravoxel incoherent motion MR imaging. Radiology 1988;168:497–505.
[5] Kim HS, Suh CH, Kim N, Choi C-G, Kim SJ. Histogram analysis of intravoxel incoherent motion for differentiating recurrent tumor from treatment effect in patients with glioblastoma: initial clinical experience. AJNR Am J Neuroradiol 2014;35:490–7. https://doi.org/10.3174/ajnr.A3719.
[6] Federau C, O'Brien K, Meuli R, Hagmann P, Maeder P. Measuring brain perfusion with intravoxel incoherent motion (IVIM): initial clinical experience. J Magn Reson Imaging 2014;39:624–32. https://doi.org/10.1002/jmri.24195.
[7] Suo S, Lin N, Wang H, Zhang L, Wang R, Zhang S, et al. Intravoxel incoherent motion diffusion-weighted MR imaging of breast cancer at 3.0 tesla: comparison of different curve-fitting methods. J Magn Reson Imaging 2015;42:362–70. https://doi.org/10.1002/jmri.24799.
[8] Fujima N, Yoshida D, Sakashita T, Homma A, Tsukahara A, Tha KK, et al. Intravoxel incoherent motion diffusion-weighted imaging in head and neck squamous cell carcinoma: assessment of perfusion-related parameters compared to dynamic contrast-enhanced MRI. Magn Reson Imaging 2014;32:1206–13. https://doi.org/10.1016/J.MRI.2014.08.009.
[9] Wood AJJ, Hiatt WR. Medical treatment of peripheral arterial disease and claudication. N Engl J Med 2001;344:1608–21. https://doi.org/10.1056/NEJM200105243442108.
[10] Peach G, Griffin M, Jones KG, Thompson MM, Hinchliffe RJ. Diagnosis and management of peripheral arterial disease. BMJ 2012;345.
[11] Norgren L, Hiatt WR, Dormandy JA, Nehler MR, Harris KA, Fowkes FGR, et al. Inter-society consensus for the management of peripheral arterial disease (TASC II). J Vasc Surg 2007;45:S5–67. https://doi.org/10.1016/j.jvs.2006.12.037.
[12] Fontaine R, Kim M, Kieny R. Surgical treatment of peripheral circulation disorders. Helv Chir Acta 1954;21:499–533.
[13] Chang H, Fitzpatrick JM. A technique for accurate magnetic resonance imaging in the presence of field inhomogeneities. IEEE Trans Med Imaging 1992;11:319–29. https://doi.org/10.1109/42.158935.
[14] Welcome to Python.org n.d. https://www.python.org/(accessed December 6, 2017).
[15] Branch MA, Coleman TF, Li Y. A subspace, interior, and conjugate gradient method for large-scale bound-constrained minimization problems. SIAM J Sci Comput 1999;21:1–23. https://doi.org/10.1137/S1064827595289108.
[16] Peterson Pearu, TB Eric Jones. SciPy: open source scientific tools for Python. http://www.scipy.org/; 2001.

[17] Hu Y-C, Yan L-F, Wu L, Du P, Chen B-Y, Wang L, et al. Intravoxel incoherent motion diffusion-weighted MR imaging of gliomas: efficacy in preoperative grading. Sci Rep 2014;4:7208. https://doi.org/10.1038/srep07208.
[18] Tofts PS, Kermode AG. Measurement of the blood-brain barrier permeability and leakage space using dynamic MR imaging. 1. Fundamental concepts. Magn Reson Med 1991;17:357–67.
[19] Dathe H, Helms G. Exact algebraization of the signal equation of spoiled gradient echo MRI. Phys Med Biol 2010;55:4231–45. https://doi.org/10.1088/0031-9155/55/15/003.
[20] Tofts PS, Brix G, Buckley DL, Evelhoch JL, Henderson E, Knopp MV, et al. Estimating kinetic parameters from dynamic contrast-enhanced T(1)-weighted MRI of a diffusable tracer: standardized quantities and symbols. J Magn Reson Imaging 1999;10:223–32.
[21] Patlak CS, Blasberg RG, Fenstermacher JD. Graphical evaluation of blood-to-brain transfer constants from multiple-time uptake data. J Cereb Blood Flow Metab 1983;3:1–7. https://doi.org/10.1038/jcbfm.1983.1.
[22] Sourbron SP, Buckley DL. Classic models for dynamic contrast-enhanced MRI. NMR Biomed 2013;26:1004–27. https://doi.org/10.1002/nbm.2940.
[23] Schabel MC. A unified impulse response model for DCE-MRI. Magn Reson Med 2012;68:1632–46. https://doi.org/10.1002/mrm.24162.
[24] Sourbron SP, Buckley DL. On the scope and interpretation of the Tofts models for DCE-MRI. Magn Reson Med 2011;66:735–45. https://doi.org/10.1002/mrm.22861.
[25] Tofts PS. Modeling tracer kinetics in dynamic Gd-DTPA MR imaging. J Magn Reson Imaging 1997;7:91–101.
[26] St Lawrence KS, Lee T-Y. An adiabatic approximation to the tissue homogeneity model for water exchange in the brain: I. Theoretical derivation. J Cereb Blood Flow Metab n.d.;18:1365–77.
[27] Brix G, Salehi Ravesh M, Zwick S, Griebel J, Delorme S, Brix G. On impulse response functions computed from dynamic contrast-enhanced image data by algebraic deconvolution and compartmental modeling. Phys Med 2012;28:119–28. https://doi.org/10.1016/j.ejmp.2011.03.004.
[28] Canny J. A computational approach to edge detection. IEEE Trans Pattern Anal Mach Intell 1986;PAMI-8:679–98. https://doi.org/10.1109/TPAMI.1986.4767851.
[29] Pluim JPW, Maintz JBA, Viergever MA. Mutual-information-based registration of medical images: a survey. IEEE Trans Med Imaging 2003;22:986–1004. https://doi.org/10.1109/TMI.2003.815867.
[30] Cover TM, Thomas JA. Elements of information theory. Wiley-Interscience; 2006.
[31] Henkelman RM. Measurement of signal intensities in the presence of noise in MR images. Med Phys 1985;12:232–3. https://doi.org/10.1118/1.595711.
[32] European Medicines Agency - Human medicines - gadolinium-containing contrast agents n.d. http://www.ema.europa.eu/ema/index.jsp?curl=pages/medicines/human/referrals/Gadolinium-containing_contrast_agents/human_referral_prac_000056.jsp&mid=WC0b01ac05805c516f (accessed December 6, 2017).
[33] Pollak AW, Meyer CH, Epstein FH, Jiji RS, Hunter JR, Dimaria JM, et al. Arterial spin labeling MR imaging reproducibly measures peak-exercise calf muscle perfusion: a study in patients with peripheral arterial disease and healthy volunteers. JACC Cardiovasc Imaging 2012;5:1224–30. https://doi.org/10.1016/j.jcmg.2012.03.022.
[34] Huegli RW, Schulte A-C, Aschwanden M, Thalhammer C, Kos S, Jacob AL, et al. Effects of percutaneous transluminal angioplasty on muscle BOLD-MRI in patients with peripheral arterial occlusive disease: preliminary results. Eur Radiol 2009;19:509–15. https://doi.org/10.1007/s00330-008-1168-6.
[35] Grözinger G, Pohmann R, Schick F, Grosse U, Syha R, Brechtel K, et al. Perfusion measurements of the calf in patients with peripheral arterial occlusive disease before and after percutaneous transluminal angioplasty using Mr arterial spin labeling. J Magn Reson Imaging 2014;40:980–7. https://doi.org/10.1002/jmri.24463.
[36] Jiji RS, Pollak AW, Epstein FH, Antkowiak PF, Meyer CH, Weltman AL, et al. Reproducibility of rest and exercise stress contrast-enhanced calf perfusion magnetic resonance imaging in peripheral arterial disease. J Cardiovasc Magn Reson 2013;15:14. https://doi.org/10.1186/1532-429X-15-14.
[37] Mostardi PM, Haider CR, Glockner JF, Young PM, Riederer SJ. High spatial and temporal resolution imaging of the arterial vasculature of the lower extremity with contrast enhanced MR angiography. Clin Anat 2011;24:478–88. https://doi.org/10.1002/ca.21124.